Journal of Sound and Vibration (1998) **217**(1), 127–143
Article No. sv981739

NON-LINEAR SPRING RESISTANCE AND FRICTION DAMPING OF FRICTIONAL CONSTRAINT HAVING TWO-DIMENSIONAL MOTION

C. H. Menq and B. D. Yang

Coordinate Metrology and Measurement Laboratory, *Department of Mechanical Engineering*, *The Ohio State University*, *Columbus*, *OH* 43210, *U.S.A.*

(*Received* 18 *December* 1997, *and in final form* 8 *May* 1998)

A model is proposed to investigate the contact kinematics of a frictional constraint experiencing two-dimensional relative motion. In this model, a contact plane is defined and its orientation is invariant. In addition, the contact normal load is assumed constant. In this study, analytical criteria are developed to determine the transitions between stick and slip which characterize how the friction force relates to the two-dimensional relative motion. Using the stick–slip transition criteria, a stick–slip diagram of elliptical motion is developed. This stick–slip diagram illustrates the fundamental characteristics of the two-dimensional contact kinematics when the relative motion has an elliptical trajectory. Fourier series expansion is employed to divide the induced periodic friction force into two components: non-linear spring resistance and friction damping. In this study, a set of non-linear functions that relate the non-linear spring resistance and friction damping to the elliptical motion are developed. It is shown that these non-linear functions can be analytically derived for the two extreme cases: circular motion and one-dimensional motion. The single-term harmonic balance scheme along with the non-linear spring resistance and friction damping of the frictional constraint then used to calculate the resonant response of a frictionally constrained two-degree-of-freedom oscillator. The accuracy of the method is demonstrated by comparing the results with those of the direct time integration method.

1. INTRODUCTION

Mechanical systems in which moving components are mutually constrained through frictional contacts often lead to complex contact kinematics. If the relative motion of the contacting surfaces follows a straight line, the motion is said to be one-dimensional [1]. This case arises from either the specific design of friction contact [2–5] or from the simplification of the analysis [6–9]. More generally, the point of contact can follow a path which is not a straight line. For the case of a periodic response, the path will form a closed loop and the relative motion is

0022–460X/98/410127 + 17 $30.00/0

said to be two-dimensional [10]. In this paper the contact kinematics of a frictional constraint experiencing two-dimensional relative motion is investigated.

The dry friction dampers used in turbomachinery to reduce the turbine blade vibration often exhibit two-dimensional contact kinematics due to the existence of the interblade phase angle [11] and/or possible multiple mode vibration [10]. This motivates the development of a two-dimensional friction force model that can be used to predict the non-linear spring resistance and friction damping of the frictional constraint so as to investigate the resonant response of a frictionally constrained structure.

An interpolation method for estimating the friction force when the friction contact undergoes two-dimensional stick–slip motion in steady state was presented in our earlier work [10]. In reference [10], analytical criteria that determine the transitions between stick and slip were not available. Therefore, the relationship between the friction force and the displacement could not be established rigorously. In section 2, a model is proposed to investigate the contact kinematics of a frictional constraint experiencing two-dimensional relative motion. In this study, analytical criteria are developed to determine the transitions between stick and slip which characterize how the friction force relates to the two-dimensional relative motion. In section 3, using the stick–slip transition criteria, a stick–slip diagram of elliptical motion is developed. This stick–slip diagram illustrates the fundamental characteristics of the two-dimensional contact kinematics when the relative motion has an elliptical trajectory. In section 4, Fourier series expansion is employed to divide the induced periodic friction force into two components: non-linear spring resistance and friction damping. In this study, a set of non-linear functions that relate the non-linear spring resistance and friction damping to the elliptical motion are developed. It is shown that these non-linear functions can be analytically derived for the two extreme cases: circular motion and one-dimensional motion. In section 5, the single-term harmonic balance scheme along with the non-linear spring resistance and friction damping of the frictional constraint is then used to calculate the resonant response of a frictionally constrained two-degree-of-freedom oscillator. The accuracy of the method is demonstrated by comparing the results with those of the direct time integration method. The conclusions are summarized in section 6.

2. TWO-DIMENSIONAL CONTACT KINEMATICS

Figure 1 depicts a model of the frictional constraint experiencing two-dimensional relative motion. In this model, a contact plane is defined and its orientation is invariant. In addition, the contact normal load is assumed constant. Based on this model, the purpose of this study is to understand how the friction force relates to the two-dimensional relative motion. Therefore, one of the two contacting surfaces can be considered as the ground. This model consists of two components: a massless elastic element accounting for the compliance of the frictional interface and a friction element obeying the Coulomb friction law. It should be pointed out that the compliance of the frictional interface can be an important parameter that controls the effectiveness of a frictional constraint when

the attenuation of resonant response is desired [8]. In this study, the flexible element is characterized by a 2×2 stiffness matrix $\mathbf{k}$, and the friction element can be modelled as, under the assumption of the Coulomb friction law, a contact point O with friction coefficient μ. In this paper, $\mathbf{u}$ denotes the input relative motion, $\mathbf{w}$ the slip motion of the contact point, and $\mathbf{f}$ the induced friction force. These vectors are all on the contact plane. The normal load n is a constant scalar. For simplicity, three dimensionless variables are defined: $\bar{\mathbf{u}} = \mathbf{ku}/\mu n$, $\bar{\mathbf{w}} = \mathbf{kw}/\mu n$ and $\bar{\mathbf{f}} = \mathbf{f}/\mu n$.

2.1. FRICTION FORCE

The dimensionless friction force, acting on the ground, can be expressed as

$$\bar{\mathbf{f}} = \bar{\mathbf{u}} - \bar{\mathbf{w}}. \tag{1}$$

When the vibratory motion is small, the contact point sticks and the friction force is proportional to the displacement $\bar{\mathbf{u}}$ with reference to $\dot{\bar{\mathbf{w}}} = \mathbf{0}$. According to the Coulomb friction law, the magnitude of the friction force is always limited by the slip load μn, therefore $|\bar{\mathbf{f}}| < 1$. During the course of vibration, the interface may reach a point where the friction force tends to exceed the slip load and begin to slip. Subsequently, the friction force remains equal to the slip load, and slip takes place along the direction of the friction force until the contact point sticks again. In other words, the stick and slip condition can be expressed as follows:

stick condition:
$$|\bar{\mathbf{f}} = \bar{\mathbf{u}} - \bar{\mathbf{u}}_0 + \bar{\mathbf{f}}_0| < 1, \qquad \dot{\bar{\mathbf{w}}} = \mathbf{0}; \tag{2}$$

slip condition:
$$\bar{\mathbf{f}} = \dot{\bar{\mathbf{w}}}/|\dot{\bar{\mathbf{w}}}|, \qquad \dot{\bar{\mathbf{w}}} \neq \mathbf{0}; \tag{3}$$

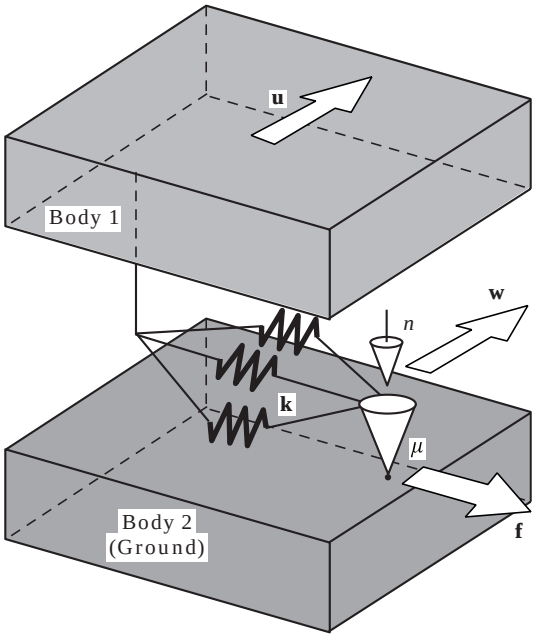

Figure 1. A model of the friction interface experiencing 2-D contact kinematics.

where $\bar{\mathbf{u}}_0$ and $\bar{\mathbf{f}}_0$ are the respective initial values of $\bar{\mathbf{u}}$ and $\bar{\mathbf{f}}$ at the beginning of the stick state.

2.2. STICK–SLIP TRANSITION

When analyzing the stick–slip behavior of a friction interface experiencing two-dimensional motion, it is essential to predict the stick–slip transition so as to accurately evaluate the induced friction force. There are two types of transition, namely stick-to-slip transition and slip-to-stick transition. The first one can be determined by the condition when the amplitude of the friction force tends to exceed the slip load. On the other hand, the criterion of the second one (slip-to-stick transition) is not as straightforward as the simple "rule of thumb" that the slip-to-stick transition occurs when the input relative motion reverses its direction. This "reversion rule" has been widely used in the case in which the interface experiencing one-dimensional relative motion [4, 8, 9, 12]. However, for the two-dimensional contact kinematics, the input relative motion follows a two-dimensional trajectory, which never actually reverses its direction but keeps moving in a closed path. In fact, the above mentioned stick and slip conditions suggest that the slip-to-stick transition can be determined when $\dot{\bar{\mathbf{w}}} = \mathbf{0}$, but how to relate $\dot{\bar{\mathbf{w}}}$ to the input relative motion $\bar{\mathbf{u}}$ needs to be further addressed.

2.2.1. *Stick-to-slip transition*

Given an initial state, $\bar{\mathbf{u}}_0$ and $\bar{\mathbf{f}}_0$, the stick-to-slip transition occurs when $|\bar{\mathbf{f}} = \bar{\mathbf{u}} - \bar{\mathbf{u}}_0 + \bar{\mathbf{f}}_0| = 1$ and $|\dot{\bar{\mathbf{f}}}| > 0$. This transition condition can be used to determine when the contact point starts to slip for any input motion $\bar{\mathbf{u}}$. When considering an elliptical relative motion, the criterion can be transformed into a quartic equation [13], whose solutions are available in the analytical form [14]. Since multiple solutions may appear, the redundant solutions can be eliminated by considering the constraint $|\dot{\bar{\mathbf{f}}}| > 0$ that guarantees the magnitude of the friction force to have a tendency to exceed the slip load. Figure 2 exemplifies graphically how the stick-to-slip transition can be obtained. In this figure, the transition angle θ_1 can be found to be the moment when the elliptical trajectory $\bar{\mathbf{u}} - \bar{\mathbf{u}}_0 + \bar{\mathbf{f}}_0$ intersects with the unit circle.

2.2.2. *Slip-to-stick transition*

During the slip state, according to the Coulomb friction law as described in equation (3), the slip velocity of the contact point $\dot{\bar{\mathbf{w}}}$ is along the direction of the friction force, i.e.,

$$\dot{\bar{\mathbf{w}}} = c\dot{\bar{\mathbf{f}}}, \qquad \text{where } c > 0. \tag{4}$$

Since the magnitude of the friction force is constant, one has

$$\bar{\mathbf{f}}^T\dot{\bar{\mathbf{f}}} = 0. \tag{5}$$

Considering equation (4) and the time differentiation of equation (1), the above equation becomes

$$\bar{\mathbf{f}}^T\dot{\bar{\mathbf{u}}} - c\bar{\mathbf{f}}^T\bar{\mathbf{f}} = 0. \tag{6}$$

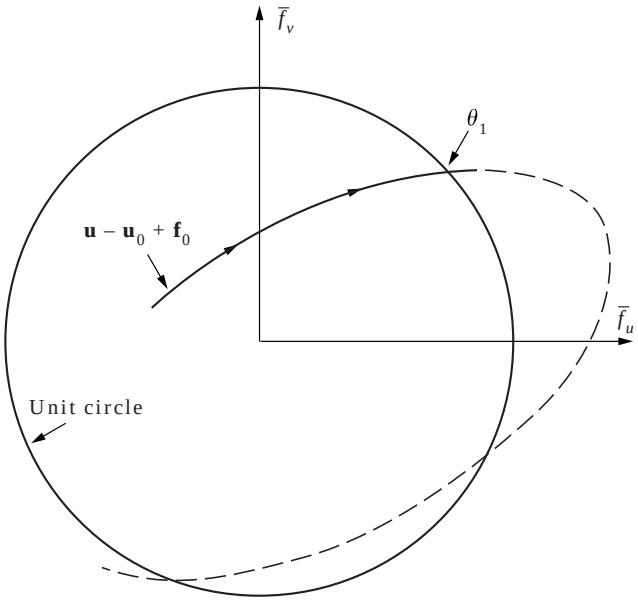

Figure 2. Stick-to-slip transition.

Since $\bar{\mathbf{f}}^T\bar{\mathbf{f}} = 1$, one can have c as follows:

$$c = \bar{\mathbf{f}}^T\dot{\mathbf{u}}. \tag{7}$$

Therefore, the slip velocity of the contact point during the slip state can be expressed as

$$\dot{\mathbf{w}} = \bar{\mathbf{f}}^T\dot{\mathbf{u}}\bar{\mathbf{f}}. \tag{8}$$

Substituting equation (8) into $\dot{\bar{\mathbf{f}}} = \dot{\mathbf{u}} - \dot{\mathbf{w}}$ yields

$$\dot{\bar{\mathbf{f}}} = \dot{\mathbf{u}} - \bar{\mathbf{f}}^T\dot{\mathbf{u}}\bar{\mathbf{f}}. \tag{9}$$

From equation (8), the slip-to-stick transition criterion $\dot{\mathbf{w}} = \mathbf{0}$ implies

$$\bar{\mathbf{f}}^T\dot{\mathbf{u}} = 0. \tag{10}$$

However, it should be noted that $\bar{\mathbf{f}}$ still remains undetermined at this stage. To obtain $\bar{\mathbf{f}}$, the initial value problem involving equation (9) and the known initial friction force at the beginning of the slip condition can be solved using a numerical integration scheme. Once the friction force is obtained, equation (10) can be used to predict the occurrence of the slip-to-stick transition.

3. STICK–SLIP DIAGRAM OF ELLIPTICAL MOTION

When the input relative motion is small, the friction contact is stuck and merely contributes a linear spring resistance. In this case the resonant response can be easily derived. When the relative motion is sufficiently large to cause slip, an analytical solution is often not available. In this case the steady state response can be determined by using either the time integration method or the harmonic balance

scheme. In this paper, the harmonic balance scheme will be employed. Therefore, it is necessary to derive the induced friction force when given an elliptical relative motion.

The dimensionless input motion is now assumed to have an elliptical trajectory. Using a local co-ordinate system based on the principal directions of the elliptical motion, the input motion can be expressed as

$$\bar{\mathbf{u}} = [a\cos\theta \quad b\sin\theta]^T \qquad \text{and} \qquad \dot{\bar{\mathbf{u}}} = [-a\sin\theta \quad b\cos\theta]^T\dot{\theta}, \tag{11}$$

where $\theta = \omega t + \phi$ and ϕ is the initial phase of the elliptical motion. When the input motion causes the friction contact to slip, the friction force can be expressed as

$$\bar{\mathbf{f}} = [\cos\varphi \quad \sin\varphi]^T \qquad \text{and} \qquad \dot{\bar{\mathbf{f}}} = [\sin\varphi \quad \cos\varphi]^T\dot{\varphi}. \tag{12}$$

Using equation (9), one can find that the changing rate of the friction force is characterized by

$$\frac{\mathrm{d}\varphi}{\mathrm{d}\theta} = \frac{a+b}{2}\cos(\theta-\varphi) - \frac{a-b}{2}\cos(\theta+\varphi). \tag{13}$$

Similarly equation (7) yields that

$$c = \omega\left[-\frac{a+b}{2}\sin(\theta-\varphi) - \frac{a-b}{2}\sin(\theta+\varphi)\right]. \tag{14}$$

Using equation (13), the induced friction force during the slip state can be calculated. Since c has to be positive during the slip state, when c crosses zero the friction contact changes from slip state to stick. The steady state friction force can be attained using a "state-by-state simulation" by calculating the stick–slip transitions sequentially. One example of the resulting friction force by the state-by-state simulation is shown in Figure 3. In this figure, the unit circle limits the range of the dimensionless friction force. The trajectory inside the unit circle represents a stick state, while the trajectory falling on the unit circle represents a slip state. The simulation starts from a stick state with zero friction force. The stick-to-slip transition θ_1 can be predicted by solving the corresponding stick-to-slip transition criterion when the elliptical trajectory $\bar{\mathbf{u}} - \bar{\mathbf{u}}_0 + \bar{\mathbf{f}}_0$ intersects with the unit circle. The simulation proceeds to a slip state until the next slip-to-stick transition θ_2 is encountered. During a slip state, equation (13) is used to calculate φ and equation (14) is used to calculate c. The slip-to-stick transition θ_2 is encountered when c crosses zero. When it happens, the simulation starts a stick state again. The simulation continues in the same matter to find the following transitions (θ_3, θ_4, . . . , etc.) until the steady state friction force is reached. As can be seen from this resulting trajectory, the steady state friction force is always obtained within a few cycles.

Three types of friction force trajectory are identified and shown in Figure 4. When the amplitude of the input relative motion is small, the interface remains stuck all the time, and as a result, the fully stuck trajectory follows an ellipse. This is shown in Figure 4(a). As the amplitude of the relative motion increases to cause

the induced friction force to exceed the slip load, slip takes place. In this case, the interface undergoes an alternating stick and slip motion and the resulting trajectory is shown in Figure 4(b). When the amplitude of the relative motion exceeds a certain level, the interface is fully slipping, and the resulting friction force has a circular trajectory. This is shown in Figure 4(c). Figure 5 shows a stick–slip diagram in terms of the two principal axes of the input elliptical motion. Since a is the length of the major principal axis, it is clear that $a \geqslant b$. In this figure, the two-dimensional motion degenerates to one-dimensional motion when $b = 0$, and becomes circular motion when $b = a$. It can be seen that the friction contact will be fully stuck when $a < 1$. If $a > 1$, the friction contact experiences an alternating stick–slip motion when b is small, however, it becomes fully slipping as b increases and exceeds a critical value. This stick–slip diagram illustrates the fundamental characteristics of the two-dimensional contact kinematics when the relative motion has an elliptical trajectory.

4. NON-LINEAR SPRING RESISTANCE AND FRICTION DAMPING

In this study, a set of non-linear functions that relate the non-linear spring resistance and friction damping to the elliptical motion are developed. It is shown that these non-linear functions can be analytically derived for the two extreme cases: circular motion and one-dimensional motion.

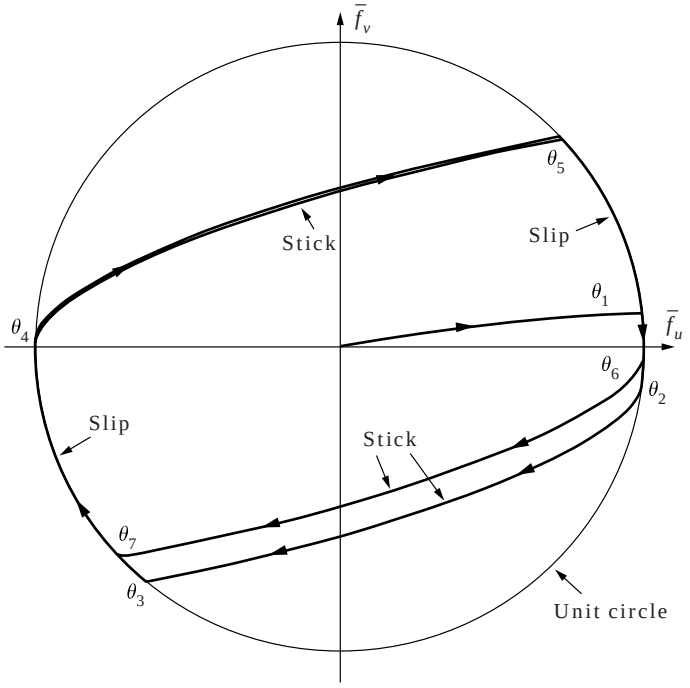

Figure 3. The resulting friction force trajectory using state-by-state simulation.

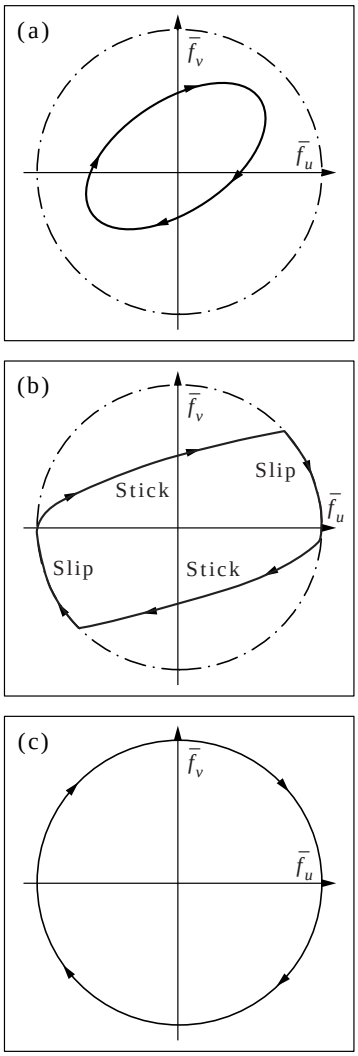

Figure 4. Three types of steady state friction force trajectories: (a) fully stuck; (b) stick–slip; (c) fully slipping.

4.1. ELLIPTICAL MOTION

Once the steady state friction force is determined, a one-term Fourier series expansion can be employed to divide the periodic friction force into two components. The first one is in phase with the input motion and provides additional spring resistance to the structure constrained by the friction contact. The second component is 90° out of phase with the input motion and adds friction damping to the structure:

$$\bar{\mathbf{f}} = \begin{bmatrix} \bar{f}^u \\ \bar{f}^v \end{bmatrix} \approx \begin{bmatrix} \bar{f}^u_s \cos\theta - \bar{f}^u_c \sin\theta \\ \bar{f}^v_s \sin\theta + \bar{f}^v_c \cos\theta \end{bmatrix}. \tag{15}$$

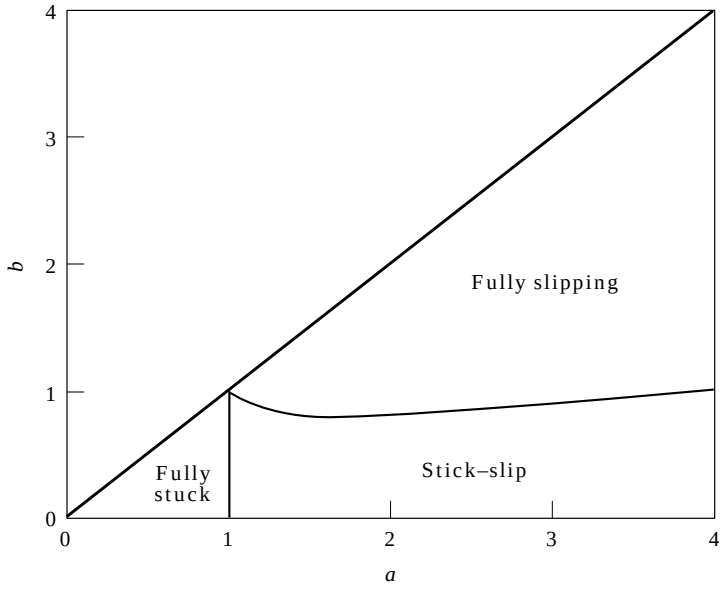

Figure 5. Stick–slip diagram.

In this expression, the u and v directions are defined along the principal major and minor axes of the dimensionless relative motion, respectively. The results of the dimensionless spring resistance ($\bar{f}_s^u$ and $\bar{f}_s^v$) and friction damping ($\bar{f}_c^u$ and $\bar{f}_c^v$) are

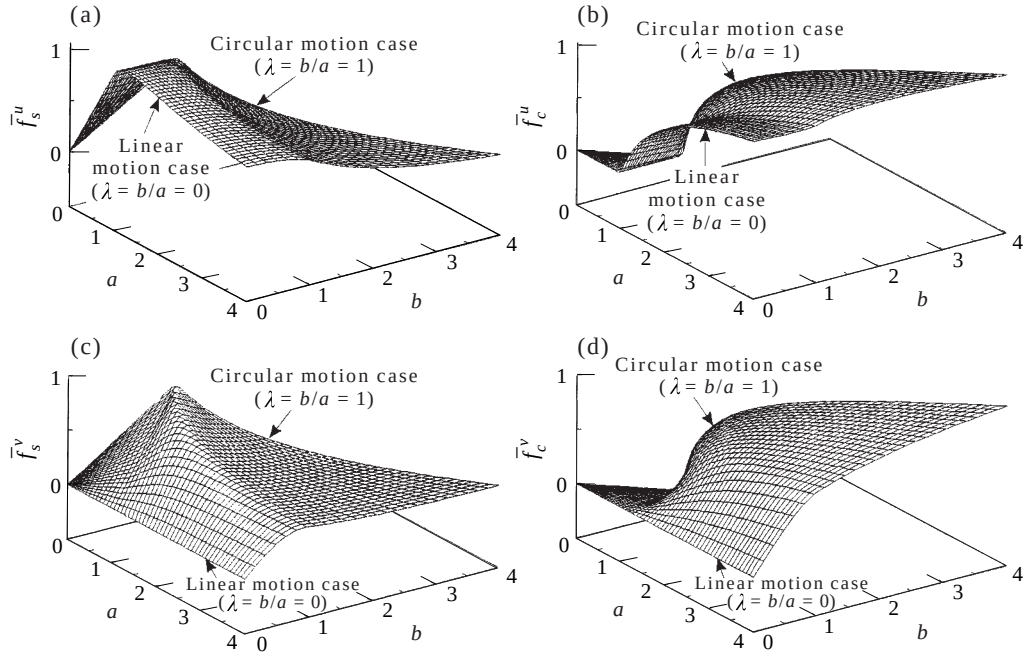

Figure 6. Dimensionless spring resistance and friction damping: (a) spring resistance in the u direction; (b) friction damping in the u direction; (c) spring resistance in the v direction; (d) friction damping in the v direction.

depicted in terms of a and b in Figure 6, in which a is the amplitude of the principal major axis, b the amplitude of the principal minor axis, and $a \geqslant b$. In the figure, the calculated values are plotted as functions of a and b that range within $0 \leqslant a \leqslant 4$ and $0 \leqslant b \leqslant a$. For each plot, there are two boundary curves corresponding to the two extreme cases. The one having $\lambda = b/a = 0$ is the case of one-dimensional motion and the other $\lambda = b/a = 1$ is of circular motion. With these dimensionless functions, the induced friction force can be estimated as

$$\mathbf{f} = \begin{bmatrix} f^u \\ f^v \end{bmatrix} \approx \mu n \begin{bmatrix} \overline{f}^u_s(a, b) \cos\theta - \overline{f}^u_c(a, b) \sin\theta \\ \overline{f}^v_s(a, b) \sin\theta + \overline{f}^v_c(a, b) \cos\theta \end{bmatrix}. \tag{16}$$

4.2. CIRCULAR MOTION

If b equals a, the elliptical motion becomes circular motion [1]. In this case, the friction contact is fully stuck when $a < 1$. If $a \geqslant 1$, the friction contact can slip and equations (13) and (14) become

$$\frac{\mathrm{d}\varphi}{\mathrm{d}\theta} = a \cos(\theta - \varphi) \tag{17}$$

and

$$c = -a\omega \sin(\theta - \varphi). \tag{18}$$

Since c has to be positive during the slip state, it can be shown that the solutions of these two equations are

$$\varphi = \theta + \cos^{-1}(1/a) \tag{19}$$

and

$$c = \omega\sqrt{a^2 - 1}. \tag{20}$$

It can be seen from equation (20) that once the friction contact begins to slip, it will continue to slip for c is always positive. In other words, the friction contact suddenly changes from fully stuck to fully slipping when a increases and exceeds 1. However, from equation (19), the phase angle between the induced friction force and the input relative motion is $\cos^{-1}(1/a)$. It indicates that when a equals 1, although the friction contact slips all the time, the phase angle equals zero and the friction force acts purely as a spring constraint. When a becomes larger, the phase angle approaches 90° and the friction force behaves like a damping force. Since the solution in equation (19) is exact, Fourier series approximation is not necessary and the induced friction force can be expressed as

$$\overline{\mathbf{f}} = \begin{bmatrix} \overline{f}^u \\ \overline{f}^v \end{bmatrix} = \begin{bmatrix} \cos\varphi \\ \sin\varphi \end{bmatrix} = \begin{bmatrix} (1/a)\cos\theta - \sqrt{1 - (1/a)^2}\sin\theta \\ (1/a)\sin\theta + \sqrt{1 - (1/a)^2}\cos\theta \end{bmatrix}. \tag{21}$$

Consequently, the dimensionless spring resistance and friction damping of circular motion have the exact expression

$$\overline{f}_s^u(a) = \overline{f}_s^v(a) = \frac{1}{a} \tag{22}$$

and

$$\overline{f}_c^u(a) = \overline{f}_c^v(a) = \sqrt{1 - (1/a)^2}. \tag{23}$$

4.3. ONE-DIMENSIONAL MOTION

If b equals zero, the elliptical motion becomes one-dimensional motion [5, 8]. From the stick–slip diagram shown in Figure 6, it is evident that a fully slipping trajectory can not happen in the case of one-dimensional motion. Again, the friction contact is fully stuck when $a < 1$. If $a \geqslant 1$, the friction contact can slip and equations (13) and (14) become

$$\frac{\mathrm{d}\varphi}{\mathrm{d}\theta} = a \sin\theta \sin\varphi \tag{24}$$

and

$$c = -a\omega \sin\theta \cos\varphi. \tag{25}$$

When the friction contact slips, according to equation (12) $\sin\varphi$ has to be zero. From equation (25), it is evident that slip-to-stick transition occurs at $\theta = 0$ and $\theta = \pi$. It is evident that the slip-to-stick transition occurs when the input relative motin reverses its direction. Since before transition occurs c has to be positive, the friction force, $\cos\varphi$, equals 1 at $\theta = 0$ and -1 at $\theta = \pi$. With this information, the induced friction force can be easily derived. Starting from $\theta = 0$, the friction contact is stuck and according to equation (2) the friction force can be expressed as

$$\overline{f}^u = a(\cos\theta - 1) + 1. \tag{26}$$

Equation (26) is valid until stick-to-slip transition occurs. Using the stick-to-slip transition condition, the transition angle can be found to be

$$\theta_1 = \cos^{-1}\left(1 - \frac{2}{a}\right). \tag{27}$$

After this transition angle, the friction force, $\overline{f}^u$, equals -1 until the friction contact sticks again at $\theta = \pi$. Similarly, the friction force for the second half cycle can be found. The resulting periodic friction force can then be decomposed into non-linear spring resistance and friction damping using a one-term Fourier series expansion. Following the expression of equation (15), one can find

$$\overline{f}_s^u(a) = \frac{a}{\pi}\left[\theta_1 - 0{\cdot}5 \sin 2\theta_1\right] \tag{28}$$

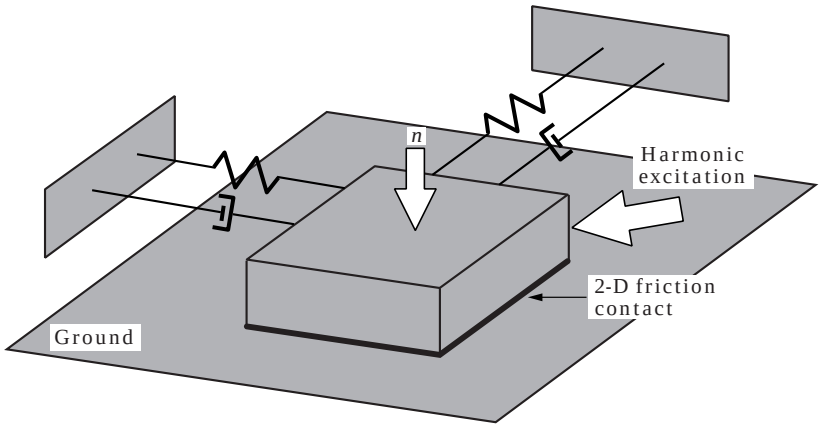

Figure 7. A two-degree-of-freedom oscillator under a friction constraint.

and

$$\bar{f}_c^u(a) = \frac{4}{\pi}\left[1 - \frac{1}{a}\right]. \tag{29}$$

It is evident that $\bar{f}^v$ equals zero for the case of one-dimensional motion.

5. FORCED RESPONSE OF A TWO-DEGREE-OF-FREEDOM OSCILLATOR

A two-degree-of-freedom oscillator, depicted in Figure 7, is employed to investigate the influence of the two-dimensional frictional constraint on the system's resonant response.

5.1. DESCRIPTION OF THE SYSTEM

The oscillator that can displace in the x–y plane is brought into contact with the ground by applied constant normal load n and is subjected to external harmonic excitation that causes vibration. Instead of using the conventional mass–spring–dashpot notation, this two-degree-of-freedom oscillator can be described by its two-mode modal information. Its system parameters along with the excitation are shown in Table 1. The friction contact between the oscillator and the ground is modelled as a Coulomb friction contact plus a flexible element, similar to the one shown in Figure 1. The parameters of the friction interface used in this investigation are: $\mu = 0{\cdot}5$ and $\mathbf{k} = \text{diagonal}\,[20\ \ 20]$.

TABLE 1

Modal information of the 2DOF oscillator and the excitation

Mode	Mass	Frequency (Hz)	Damping ratio	Mode shape	Excitation
1	1·0	0·9	0·02	$(1\ \ 1)^T$	$1{\cdot}0\angle 0^\circ$
2	1·0	1·1	0·02	$(1\ \ -1)^T$	$1{\cdot}0\angle 0^\circ$

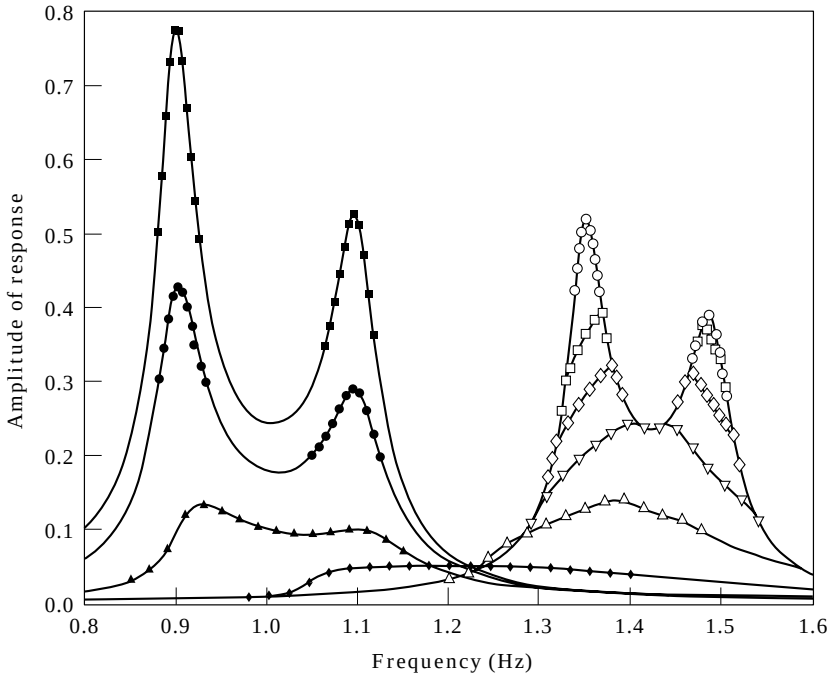

Figure 8. Resonant responses of the 2DOF oscillator. Values of n: ■, 0·0; ●, 0·5; ▲, 1·0; ◆, 2·0; △, 5·0; ▽,10; ◇, 15; □, 20; ○, fully stuck.

5.2. FORCED RESPONSE

It is assumed that after a sufficiently long time, a steady periodic motion with the same period as that of the excitation is established. The single-term harmonic balance scheme [4, 15] along with those non-linear functions that represent the non-linear spring resistance and friction damping of the frictional constraint is used to calculate the resonant response of the two-degree-of-freedom oscillator. Using this approach, the non-linear differential equations of the system's motion are converted to a set of non-linear algebraic equations in terms of the unknown motion's amplitude and phase. These non-linear algebraic equations are then solved iteratively to yield solutions.

The predicted resonant response of this system is shown in Figure 8 as continuous curves, each of which corresponds to a specific normal load. Since the characteristics of the resulting response along the y direction is similar to that of the response along the x direction, only the amplitude of the response along the x direction is shown in this figure. In the figure, one can observe two limit cases, namely the zero-normal-load case and the fully-stuck case. Both cases are linear for the non-linear damping does not appear in the analysis. The zero-normal-load case occurs when the normal load is not present and therefore the frictional interface is not in effect. Two resonant frequencies that correspond to the natural frequencies of the system can be clearly seen. When the normal load exceeds a certain value ($n > 30$ in this example), the interface remains fully stuck. In this case, the friction interface does not dissipate energy but provides additional stiffness that arises from the compliance of the interface to the system to cause

higher resonant frequencies. This "frequency shifting" can be seen as the natural frequencies of the two vibration modes of the system (0·9 and 1·1 Hz) are shifted to 1·35 and 1·49 Hz, respectively. In between these two linear cases, the resonant frequency increases as the normal load increases, and the resonant response is damped as a result of the slip motion occurring in the friction interface. As $n = 2$, the effectiveness of the frictional constraint reaches the maximum.

From the results, it can also be observed that most of the responses consist of two peaks that associate with the two vibration modes, except for the cases of $n = 2$ and 5. As a matter of fact, it can be found that in the vicinity of the optimal normal load, the response only contains one resonance, indicating that the two vibration modes are strongly coupled together. In these situations, the two-dimensional motion is expected to be significant; this argument can be validated by examining the aspect ratio, $\lambda = b/a$, of the resulting elliptical trajectory. For each response curve in Figure 8, the aspect ratios at the peaks are shown in Table 2. For example, when $n = 5$, the peak occurs at $\omega = 1{\cdot}39$ Hz and the corresponding aspect ratio is 0·78. The results indicate that, in general, when the friction interface is highly effective, it may not be a good idea to assume that the relative motion at the friction is one-dimensional.

5.3. COMPARISON OF THE HARMONIC BALANCE METHOD AND THE TIME INTEGRATION METHOD

The harmonic balance method approximates the induced periodic friction force by truncating its Fourier series after the fundamental terms to calculate the steady state solutions. Although this procedure is computationally efficient, its accuracy needs be validated. This can be done by comparing the approximate solutions with those from the direct time integration method. In Figure 8, the discrete data points represent the time integration solutions. All the comparisons are made in the frequency range near resonance.

TABLE 2

Aspect ratio of the resulting elliptical trajectory

Normal load	λ	
0	0·08 (0·90)[a]	0·12 (1·10)
0·5	0·14 (0·91)	0·23 (1·10)
1	0·32 (0·93)	0·42 (1·10)
2	0·35 (1·26)[b]	
5	0·78 (1·39)	
10	0·34 (1·40)	0·29 (1·44)
15	0·17 (1·38)	0·24 (1·47)
20	0·16 (1·37)	0·19 (1·48)
>30	0·12 (1·35)	0·16 (1·49)

[a] The numbers in the parentheses are the resonant frequencies in Hz.

[b] The location of the resonance is unclear due to the absence of a notable peak. The aspect ratio is selected to be the maximum over the range of the flat response.

For the zero-normal-load and fully-stuck cases, the exactness of the approximate solutions is expected because the system is linear under both conditions. When the problem becomes non-linear for the cases between the two limiting cases, the approximate procedure still shows very good accuracy. There are two reasons. First, the fact that the resulting periodic friction force for two-dimensional motion is closer to pure harmonic force when compared to that of one-dimensional motion. Second, the super-harmonic terms of the periodic friction force is attenuated by the low-pass filtering nature of the two-degree-of-freedom oscillator. As a result, the resulting motion has a trajectory closely resembling an ellipse. However, when dealing with more complex systems the use of multi-harmonic balance method may be necessary [16].

6. CONCLUSIONS

A model is proposed to investigate the contact kinematics of a frictional constraint experiencing two-dimensional relative motion. In this model, a contact plane is defined and its orientation is invariant. In addition, the contact normal load is assumed constant. This model consists of two components: a massless elastic element accounting for the compliance of the frictional interface and a friction element obeying the Coulomb friction law. In this study, analytical criteria are developed to determine the transitions between stick and slip which characterize how the friction force relates to the two-dimensional relative motion. Using the stick–slip transition criteria, a stick–slip diagram of elliptical motion is developed. This stick–slip diagram illustrates the fundamental characteristics of the two-dimensional contact kinematics when the relative motion has an elliptical trajectory.

Fourier series expansion is employed to divide the induced periodic friction force into two components. The first one is in phase with the input motion and provides additional spring resistance to the structure constrained by the friction contact. The second component is 90° out of phase with the input motion and adds friction damping to the structure. In this study, a set of non-linear functions that relate the non-linear spring resistance and friction damping to the elliptical motion are developed. It is shown that these non-linear functions can be analytically derived for the two extreme cases: circular motion and one-dimensional motion.

The single-term harmonic balance scheme along with the non-linear spring resistance and friction damping of the frictional constraint is then used to calculate the resonant response of a frictionally constrained 2DOF oscillator. The system was selected to have two closely spaced natural frequencies, which simulate the coupling of the bending and torsional modes of a turbine blade. It was found that the aspect ratio of the elliptical response trajectory is significantly large, especially when the frictional constraint is highly effective. The accuracy of the method is demonstrated by comparing the results with those of the direct time integration method.

ACKNOWLEDGMENT

This material is based on work supported by the GUIde Consortium and the U.S. Air Force under contract no. F33615-96-C-2664. Any opinions, findings, and conclusions or recommendations expressed in this material are those of the authors and do not necessarily reflect the views of the GUIde Consortium or the Air Force.

REFERENCES

1. J. H. Griffin and C. H. Menq 1991 *Transactions of the American Society of Mechanical Engineers*, *Journal of Vibration and Acoustics* **113**, 225–229. Friction damping of circular motion and its implications to vibration control.
2. T. M. Cameron, J. H. Griffin, R. E. Kielb and T. M. Hoosac 1990 *Transactions of the American Society of Mechanical Engineers*, *Journal of Vibration*, *Acoustics*, *Stress*, *and Reliability in Design* **112**, 175–182. An integrated approach for friction damper design.
3. E. H. Dowell and H. B. Schwartz 1983 *Journal of Sound and Vibration* **91**, 255–267. Forced response of a cantilever beam with a dry friction damper attached, part I: theory.
4. C. H. Menq and J. H. Griffin 1985 *Transactions of the American Society of Mechanical Engineers*, *Journal of Vibration*, *Acoustics*, *Stress*, *and Reliability in Design* **107**, 19–25. A comparison of transient and steady state finite element analyses of the forced response of a frictionally damped beam.
5. E. J. Williams and S. W. Earles 1974 *Transactions of the American Society of Mechanical Engineers*, *Journal of Engineering for Industry* **96**, 471–476. Optimization of the response of frictionally damped beam type structures with reference to gas turbine compressor blading.
6. J. P. Den Hartog 1931 *Transactions of the American Society of Mechanical Engineers* **APM-53-9**, 107–115. Forced vibration with combined Coulomb and viscous friction.
7. A. A. Ferri 1996 *Transactions of the American Society of Mechanical Engineers*, *Journal of Vibration and Acoustics* **117**(B), 196–206. Friction damping and isolation systems.
8. J. H. Griffin 1980 *Transactions of the American Society of Mechanical Engineers*, *Journal of Engineering for Power* **102**, 329–333. Friction damping of resonant stresses in gas turbine engine airfoils.
9. C. H. Menq, J. H. Griffin and J. Bielak 1986 *Transactions of the American Society of Mechanical Engineers*, *Journal of Engineering for Gas Turbines and Power* **108**, 300–305. The influence of a variable normal load on the forced vibration of a frictionally damped structure.
10. C. H. Menq, P. Chidamparam and J. H. Griffin 1991 *Journal of Sound and Vibration* **144**, 427–447. Friction damping of two-dimensional motion and its application in vibration control.
11. B. D. Yang and C. H. Menq 1997 *Transactions of the American Society of Mechanical Engineers*, *Journal of Engineering for Gas Turbines and Power* **119**, 958–963. Modeling of friction contact and its application to the design of shroud contact.
12. A. V. Srinivasan and D. G. Cutts 1983 *Transactions of the American Society of Mechanical Engineers*, *Journal of Engineering for Power* **105**, 332–341. Dry friction damping mechanisms in engine blades.
13. B. D. Yang 1996 *Ph.D. Dissertation*, *Department of Mechanical Engineering*, *The Ohio State University*. Contact kinematics of friction interfaces and applications to the prediction of resonant response of frictionally constrained turbine blades.
14. S. Neumark 1965 *Solution of Cubic and Quartic Equations*. New York: Pergamon Press.

15. K. Y. Sanliturk and D. J. Ewins 1996 *Journal of Sound and Vibration* **193**, 511–523. Modelling two-dimensional friction contact and its application using harmonic balance method.
16. J. Guillen and C. Pierre 1996 *Proceedings of the* 1996 *ASME IMECE*, *Atlanta*, *GA*, 17–22 *November*. Analysis of forced response of dry-friction damped structural system using an efficient hybrid frequency–time method.